Influence of hydrophobic effects on streaming potential

Jeevanjyoti Chakraborty[1] and Suman Chakraborty[1,2,*]
[1]*Advanced Technology Development Centre, Indian Institute of Technology Kharagpur, Kharagpur-721302, India*
[2]*Mechanical Engineering Department, Indian Institute of Technology Kharagpur, Kharagpur-721302, India*
(Received 2 July 2013; published 15 October 2013)

We study the influence of hydrophobic effects on streaming potential mediated flow through a narrow confinement. In a clear departure from the approach used in prior works, we use a phase-field model to capture the hydrophobicity-induced depletion in the near wall region, and express the variation of viscosity and permittivity across the interfacial layer in terms of the phase-field variable. We then use these in the determination of the flow velocity, and highlight the sensitive interplay between the intrinsic length scale of the electrical double layer and that of the depletion in terms of the variations of an effective normalized viscosity that captures the electroviscous effect. We expect that this work will be an important step forward in the realistic continuum modeling of interfacial physics in the particular context of streaming potential mediated flows.

DOI: 10.1103/PhysRevE.88.043007 PACS number(s): 47.61.−k

I. INTRODUCTION

Streaming potential significantly influences pressure-gradient driven flows, especially in narrow confinements. The genesis of the streaming potential lies in the establishment of an electrified interface between a substrate and its incipient fluid. Such an electrified interface consists of a charged surface and a distribution of ionic species in its immediate vicinity; together they are referred to as the electrical double layer (EDL). The ions having the same charge as that of the surface are called counterions while the others are called the coions. The advection of these ionic species with the pressure-gradient driven flow gives rise to an electric current (streaming current) if there is a return path for the charges (closed circuit situation), or an electrical potential (which is called the streaming potential) if the sensing electrodes are connected to a high-input impedance voltmeter (open circuit situation). It is only after an initial transient period that a dynamic equilibrium is established, when there is zero net ionic current. The potential difference measured across the flow conduit in this condition is called the streaming potential [1]. This has a number of practical applications in diverse areas ranging from colloid science (for zeta potential measurements) [2,3], and geophysics [4–7] to physiology [8–10] and membrane technology [11,12]. The influence of streaming potential has also been studied in the context of electroviscous effects and electrokinetic lift [13–22]. For lab-on-a-chip technology, streaming potential has also been actively investigated for the fabrication of nanochannel batteries as miniaturized energy conversion systems [23–29].

It is well known that even without the streaming potential effects, as the characteristic dimensions of the confinements through which such pressure-gradient driven flows occur go down to the micron, submicron, and ultimately to the nanometer regime, the hydraulic resistances become increasingly stronger. This is because the hydraulic resistance is proportional to the inverse of the fourth power of the characteristic dimension [30]. Such resistances may be overcome to a considerable extent through the use of surfaces made of hydrophobic materials. Even when overcoming the resistances is not the primary motivation, the materials used to fabricate the microfluidic devices do often possess a hydrophobic nature. Thus, it is important to understand the effects stemming from such hydrophobic materials and to incorporate them properly in mathematical models.

It is a common practice to model the hydrodynamics in the presence of hydrophobic effects through the use of a Navier slip coefficient at the confining boundaries to represent the relevant hydrodynamic boundary conditions [31–35]. Such conditions have been termed as "apparent slip" in the literature because the classical no-slip boundary condition may still remain valid at the solid boundary [31]. To understand the origin of this apparent slip, we need to understand the mechanism starting from the origin of the hydrophobic effect itself.

The physical origin of the hydrophobic effects has been argued in the scientific community for a long time. Despite ongoing debates over the intricate details, it is generally agreed upon that hydrophobic effects induce the formation of a depleted region in the liquid adjacent to the wall [36–48]. This is because molecules of water (considering the most common and technologically important instance of a flow medium) are more entropically favored to form hydrogen bonds with themselves than with the hydrophobic surfaces. In reality, therefore, it is the higher affinity for water molecules for themselves and not any explicit repulsion from the surfaces (as the term "phobic" might misleadingly suggest) which leads to the formation of the depleted region [49]. This wall-adjacent depleted region is what acts as a smoothening blanket preventing the liquid flow to be inhibited by the surface asperities, if any.

It is the smooth sailing of the bulk liquid over an ultrathin cushion of the depleted phase (typically spanning over a length scale of 10 nm) that gives rise to the apparent slip. It is important to appreciate, however, that the use of the Navier slip coefficient betokens an inability to resolve the steep velocity gradients within the depleted phase. Such a practice involves the extrapolation of velocity profiles obtained in the liquid layer above the depleted region down and beyond the true boundary resulting thereby in an artificial (or,

*Corresponding author: suman@mech.iitkgp.ernet.in

apparent) deviation from the no-slip boundary condition that nevertheless prevails in reality at the wall.

The influence that such hydrophobicity mediated effects has in micro- and nanoscale flows is particularly strong in the case of electrokinetic flows. This is because the typical length scale of the EDL matches well with that of the depleted phase, leading, in turn, to possibilities of intriguing interplays between these effects. Recognizing this, huge augmentations in electro-osmotic transport velocities have been reported when walls are hydrophobic [50–64]. The possibilities of exploiting such hydrophobicity-induced slip in enhancing electrokinetic energy conversion efficiencies have also been reported [65–67].

As far as the continuum approaches in this reported literature are concerned, the boundary conditions have been invariably represented through the specification of a slip length (which is nothing but the Navier slip coefficient). This slip length is itself estimated by a two-layer model that has been extensively investigated by Tretheway and Meinhart [68]. The discreteness of the two layers in this model indeed provides a convenient mathematical framework. However, the true picture of the depletion getting progressively (and smoothly) weaker with increasing distance from the wall is unfortunately lost in the mathematical convenience of these discrete layers.

In a distinctive departure from this approach, Chakraborty *et al.* [69], building on earlier works of Chakraborty [54,70], presented a phase-field model which is not based on the consideration of predefined discrete layers. They compared the results of hydrophobicity affected electro-osmotic flow modeled using this phase-field approach with those of the two-layer model. In this phase-field model, a free-energy minimization approach is employed. The distribution of the phase-field variable termed the "order parameter" determines the relative phase distribution across a smooth profile in a thermodynamically consistent manner. Crucially, this phase-field parameter is used to describe the effective interfacial properties, namely, the viscosity and the electrical permittivity, instead of preassigning them with discrete values corresponding to either a liquid or a depleted phase. Additionally, this phase-field model allows us to relate the contact angle directly with the degree of depletion.

In the work we present here, we use the aforementioned phase-field model for streaming potential mediated flows. Notably, we consider the smooth variation of viscosity and permittivity profiles in the determination of the streaming potential mediated flow velocity. The remaining part of this article is organized as follows. In Sec. II A, we present the phase-field model for the description of the interfacial structure in terms of the profile of the order parameter variable. We then express the variation of the viscosity and the permittivity as a linear function of the order parameter profile. In Sec. II B, we use the profiles obtained for the viscosity and the permittivity for determining the streaming potential field, and the flow velocity arising as a combined consequence of the pressure-gradient driven and the induced streaming potential. We identify an effective normalized viscosity to represent the overall flow character. In Sec. III, we compare different flow situations in terms of this effective normalized viscosity, and in doing so delineate the intricate interplay between the length scale of the EDL and the length scale of the depleted region. We also highlight the influence that the strength of the hydrophobicity has on the overall flow character by studying the variation with different contact angles. In Sec. IV, we draw conclusions based on our findings reported in this work.

II. MODEL DESCRIPTION

We consider the model problem of streaming potential mediated flow of a binary electrolyte with symmetric valences of the cations $(+)$ and the anions $(-)$ through a slit channel of height $2H(0 \leqslant y \leqslant 2H)$, x being the axial direction, and y being the direction transverse to the walls. A pressure gradient applied across the length of the channel establishes a unidirectional flow through it. The consequent streaming of the ions induces a backstreaming potential so that the resultant flow is a combined consequence of the pressure gradient and the electric field associated with the streaming potential. The electrical permittivity and the dynamic viscosity which are necessary for the mathematical description of the hydrodynamics vary along the y direction because of the depletion in the liquid adjacent to the hydrophobic wall. We capture this variation based on the distribution of an order parameter variable, which, in turn, is resolved by a phase-field model. In the following we describe this phase-field model.

A. Phase-field model

The understanding which motivates the use of the phase-field model is that the depletion of solvent molecules in the vicinity of a hydrophobic substrate is basically a phase-separation phenomenon of a single component fluid into its vapor and liquid phases. The fluid is considered to be a binary mixture of liquid and vapor phases, and this undergoes a demixing process under the influence of hydrophobic effects. We track the spatial variation of the composition of this binary mixture with an order parameter variable $\phi = (n_1 - n_2)/(n_1 + n_2)$ where n_i are the number densities of the two separating phases. In our study, $\phi = -1$ represents the bulk liquid phase and $\phi = 1$ represents the vapor phase, with the consideration that the average location of a smeared boundary between the two is located at the position corresponding to $\phi = 0$.

For the phase-field model development, we closely follow the work of Andrienko *et al.* [71] and Chakraborty *et al.* [69] using the same underlying restrictions and assumptions, among which the most significant artifice involves calculating the equilibrium order parameter variation assuming that the flow does not disturb that variation. The description of the demixing thermodynamics is initiated by first considering a free-energy functional which represents the excess Ginzburg-Landau free energy for a binary mixture, and is given by [72]

$$\Delta\Omega(\phi) = \int_0^\infty \left[\frac{k}{2}\left(\frac{d\phi}{dy}\right)^2 + \Delta\omega(\phi)\right]dy + \Psi_S, \qquad (1)$$

where $\Delta\omega(\phi) = \omega(\phi) - \omega(\phi_0) - (\phi - \phi_0)(\partial\omega/\partial\phi)_{\phi_0}$ is the free energy required to produce a unit volume of uniform fluid of composition ϕ from a large reservoir at composition ϕ_0. Here, $0.5k(d\phi/dy)^2$ is the penalty for the presence of the interfacial gradient, and Ψ_S is the surface energy that accounts

for the interactions between the substrate and the fluid. Noting that for the two phases (liquid and vapor) to coexist there should be two minima in the free energy, we select a double-well shaped form of $\Delta\omega$ following Chakraborty [70] and Badalassi *et al*. [73]:

$$\Delta\omega = \frac{B}{4}\left(\phi - \sqrt{\frac{A}{B}}\right)^2\left(\phi + \sqrt{\frac{A}{B}}\right)^2, \tag{2}$$

where A and B are two positive constants such that $A, B \sim k_B T_C$ with T_C being the critical temperature for the liquid-vapor coexistence [70]. The double-well shape is clearly shown by this form of $\Delta\omega$, and the minima occur at $\phi_{eq} = +\sqrt{A/B},\ -\sqrt{A/B}$, which represent, respectively, the bulk order parameter values for the vapor and the liquid.

We note that the requirement of having two minima is a fundamental one in demixing phenomena because it is a necessity for the existence of two stable phases. The double-well potential provides the simplest realization (in mathematical terms) of such a requirement. The basis of the double-well potential lies in the van der Waals equation of state. In the context of phase-separation problems including liquid-vapor phase separation, this double-well form has been a preferred choice in many previous works [74–84]. Of course, to take into account a generic demixing phenomenon, other forms of the potential also exist in the literature, and a comprehensive discussion of such forms is presented by Chen [85]. Interestingly, even in this comprehensive review [85], the alternative forms of the potential are presented as variations on the double-well potential.

In our subsequent analysis, we adopt the principle of free-energy minimization to obtain an equilibrium order parameter profile, which we then apply to determine the streaming potential fluid flow. We use the equilibrium order parameter profile with the understanding that the unidirectional flow does not disturb this profile. Such an understanding follows immediately from the translational invariance of the conditions on the wall (which are perfectly parallel to each other), and is not dependent on any "weak flow" consideration.

Towards a full-fledged description of the interfacial structure, we note that the minimization of the free-energy functional Eq. (1) results in the following Euler-Lagrange equation:

$$\frac{d\Delta\omega}{d\phi} - \frac{d}{dy}\left[\frac{k}{2}\frac{d}{d\phi'}\left\{\left(\frac{d\phi}{dy}\right)^2\right\}\right] = 0, \tag{3}$$

so that

$$\Delta\omega = \frac{k}{2}\left(\frac{d\phi}{dy}\right)^2 + \text{constant}, \tag{4}$$

together with the boundary condition at $y = 0$:

$$\frac{d\Psi_S}{d\phi} - \frac{d}{d\phi'}\left(\frac{k}{2}\phi'^2\right) = 0.$$

This implies

$$\frac{d\Psi_S}{d\phi} - k\left.\frac{d\phi}{dy}\right|_{y=0} = 0. \tag{5}$$

In the bulk, $\Delta\omega = d\phi/dy = 0$, so that from Eq. (4), we have

$$\Delta\omega = \frac{k}{2}\left(\frac{d\phi}{dy}\right)^2,$$

or,

$$\frac{d\phi}{dy} = \pm\sqrt{\frac{2\Delta\omega}{k}}. \tag{6}$$

We obtain the profile for the order parameter from Eqs. (3) and (5). If we are to use the boundary condition given by Eq. (6), we need a specification of Ψ_S in terms of the short-range surface field and the surface enhancement parameters [86]. However, here we take a different approach following Chakraborty [70] and Chakraborty *et al*. [69] in order to make the interfacial electrohydrodynamics to be explicitly dependent on the substrate wettability. This necessitates establishing a link between the interfacial order parameter variations with the contact angle, θ_w. It is important to note here that the contact angle is simply a means to characterize the hydrophobicity of the substrate. This is the contact angle that would have been formed had we placed a droplet of the same liquid on that same substrate.

We note that the equilibrium free energy is nothing but the minimum value of the functional Eq. (1). Thus,

$$\gamma = \Omega_{\min} = \Psi_S + \int_{y_1}^{y_2}\frac{k}{2}\left(\frac{d\phi}{dy}\right)^2 2dy. \tag{7}$$

Changing the variable of integration from y to ϕ, we get

$$\begin{aligned}\gamma &= \Psi_S + \int_{\phi_S}^{\phi_0}\left(\frac{d\phi}{dy}\right)^2\frac{dy}{d\phi}d\phi \\ &= \Psi_S + \int_{\phi_S}^{\phi_0}\sqrt{2k\Delta\omega}d\phi.\end{aligned} \tag{8}$$

This allows us to express the surface free energies of the solid-vapor, solid-liquid, and liquid-vapor for a droplet-solid-vapor system as

$$\gamma_{sv} = \Psi_S + \int_{\beta}^{\phi_S}\sqrt{2k\Delta\omega}d\phi, \tag{9a}$$

$$\gamma_{sl} = \Psi_S + \int_{\phi_S}^{-\beta}\sqrt{2k\Delta\omega}d\phi, \tag{9b}$$

$$\gamma_{lv} = \int_{\beta}^{-\beta}\sqrt{2k\Delta\omega}d\phi. \tag{9c}$$

Importantly, no solid surface contributions feature in Eq. (9c). Now, following Pismen and Pomeau [87], we use the celebrated Young's equation for the contact angle, as given by $\cos\theta_w = (\gamma_{sv} - \gamma_{sl})/\gamma_{lv}$, to obtain

$$\cos\theta_w = \frac{\phi_S^3 - 3\beta^2\phi_S}{2\beta^3}, \tag{10}$$

where $\beta = \sqrt{A/B}$. Thus, the boundary condition at the wall, $y = 0$, becomes

$$\phi|_{y=0} = \phi_S = g\left(\theta_w; \beta\right), \tag{11}$$

where g is a function of the contact angle θ_w and the parameter β.

We may now obtain the profile of the phase-field variable from Eq. (3). Together with the form of $\Delta\omega$ adopted in Eq. (2), we then have

$$\frac{d^2\phi}{d\bar{y}^2} - \frac{BH^2}{k}(\phi^2 - \beta^2)\phi = 0. \tag{12}$$

where $\bar{y} = \frac{y}{H}$. For the boundary conditions, we have Eq. (11) and the bulk condition:

$$\phi(\bar{y} = 1) = -\beta. \tag{13}$$

We note that $k \sim B\xi^2$ where ξ is a measure of the interfacial thickness (up to a multiplicative constant). Then, the coefficient of the nonlinear term in Eq. (12) becomes $C^2 = H^2/\xi^2 \gg 1$. In an alternative notation, if we use $\epsilon = 1/C \ll 1$, Eq. (12) is clearly perceived to be in the form of a singular perturbation problem, where the physical manifestation of the mathematical "boundary layer" is through the interfacial layer where the depletion occurs. The interfacial thickness is clearly $O(\epsilon)$, and it is important to understand that the boundary condition given by Eq. (13) is valid for small ϵ only. We solve Eq. (14) using a control volume based finite difference approach, together with a continuation technique [88] to overcome the difficulties associated with $\varepsilon \ll 1$ or, equivalently $C \gg 1$.

Having obtained the profile for the order parameter variable, we now describe the interfacial variations of the viscosity and the permittivity in terms of ϕ. Without sacrificing the essential physics, we adopt a simple linearized functional dependence, as described below:

$$\varepsilon = \varepsilon_v \frac{1+\phi}{2} + \varepsilon_l \frac{1-\phi}{2}, \tag{14}$$

$$\eta = \eta_v \frac{1+\phi}{2} + \eta_l \frac{1-\phi}{2}. \tag{15}$$

In this context, we mention that the dynamic viscosity and the electrical permittivity of the solvent are both material properties, and these are but an upscaled continuum level manifestation of the mechanical and electrical interactions among the solvent molecules. Therefore, it is reasonable to expect that these properties will have a direct dependence on the actual number of molecules present. From the perspective of our phase-field formalism, the order parameter variable represents the relative distribution of the number density of the liquid and "depleted liquid" phases of the same fluid molecules. Thus, it stands to reason that both the dynamic viscosity and the electrical permittivity of the fluid should be proportional to the variation of this order parameter variable. The linear variation we adopt in Eqs. (14) and (15) ensures that the essence of the variations in the number density (captured by the order parameter variable) is captured directly in the variation of these two physicochemical properties of the fluid. Such linear form has also been used in previous works (see, for instance, the works by Andrienko *et al.* [71], Ding and Spelt [89], Ding *et al.* [90], Borcia and Bestehorn [91], Park *et al.* [92], and Chakraborty *et al.* [69]). If instead, we were to choose any nonlinear dependence, it would necessarily imply the imposition of *ad hoc* variations digressing from the underlying variations in the fluid. We also note that the profile of the permittivity obtained thus is qualitatively similar to the sigmoidal variation with spatial coordinate as *assumed* by Le and Zhang [93]. Needless to say, the permittivity variation (as we consider here) does indeed stand on some physically justifiable ground, and, hence, is more natural in contrast to the form assumed by Le and Zhang [93]. An added feature of our approach is that the variation of ε has an explicit dependence on the degree of substrate wettability (through the specification of θ_w). Nevertheless, we do note that both these variations may be found to be practically superimposed on each other through suitable matching of ancillary parameters. In this context, we also note that the decrements in permittivity values with solvent depletion in the proximity of hydrophobic substrates have been extensively discussed by Mishchuk [94,95].

B. Model of the streaming potential flow

The potential distribution $\psi(y)$ is determined from the Poisson-Boltzmann formalism described with two critical differences from the traditional approach. First, the permittivity ε is now considered as a function of y. Second, the depletion is considered to have an explicit influence on the electrochemical potential (setting the gradient of which to zero determines the ionic number density profiles), and this influence is captured through an extra "potential" term that is dependent on the local fluid density, following Joly *et al.* [52]: $\mu_\pm = k_B T \ln n_\pm \pm ze\psi + V_{\text{ext}}$, where $V_{\text{ext}} = -k_B T \ln \frac{\rho(z)}{\rho_l}$, with $\rho(z)$ being the local fluid density, and ρ_l being the bulk value of the liquid density (far from the wall). The physical origin of this simple modification is based on the understanding that the distribution of the ionic species is not only a function of the electrical interactions but is also dependent on the fluid number density distribution itself. This fluid distribution represented by the local density varies linearly with the order parameter too so that $\frac{\rho(z)}{\rho_l} = \frac{1+\phi}{2}\rho_{\text{ratio}} + \frac{1-\phi}{2}$ (where ρ_{ratio} is the ratio of the bulk value of the vapor density to that of the liquid density). From this particular form of the electrochemical potential, we obtain a modified version of the Poisson-Boltzmann equation as

$$\frac{\partial}{\partial y}\left(\varepsilon \frac{\partial \psi}{\partial y}\right) = 2n_0 ez \frac{\rho(z)}{\rho_l} \sinh\left(\frac{ez\psi}{k_B T}\right), \tag{16}$$

where n_0 is the bulk value of the number density of the ions, e is the elementary charge, z the valence ($z_+ = -z_- = z$), k_B the Boltzmann constant, and T the absolute temperature. We use the nondimensionalization scheme:

$$\tilde{y} = \frac{y}{H}, \quad \tilde{\psi} = \frac{ez\psi}{k_B T}, \quad \tilde{\varepsilon} = \frac{\varepsilon}{\varepsilon_l}, \tag{17}$$

so that Eq. (16) becomes

$$\frac{\partial}{\partial \tilde{y}}\left(\tilde{\varepsilon} \frac{\partial \tilde{\psi}}{\partial \tilde{y}}\right) = K^2 \gamma \sinh(\tilde{\psi}), \tag{18}$$

where $K = H/\lambda_l$ with $\lambda_l = \sqrt{\varepsilon_l k_B T/2n_0 e^2 z^2}$ being the Debye screening length based on the bulk liquid permittivity value, and $\gamma = \rho(z)/\rho_l$. Equation (18) is to be solved with the boundary conditions

$$\tilde{\psi} = \tilde{\zeta} \quad \text{at} \quad \tilde{y} = 0, \quad \text{and} \quad \frac{\partial \tilde{\psi}}{\partial \tilde{y}} = 0 \quad \text{at} \quad \tilde{y} = 1. \tag{19}$$

A finite volume based numerical approach is used to obtain the profile for $\tilde{\psi}$ [96]. The hydrodynamics is determined by

the equation

$$0 = -\frac{dp}{dx} + \frac{\partial}{\partial y}\left(\eta\frac{\partial u}{\partial y}\right) + \rho_e E_S, \tag{20}$$

where ρ_e is the charge density and is given by the Poisson equation as $\rho_e = -\partial_y(\varepsilon\partial_y\psi)$, and E_S is the streaming potential (yet to be determined). Integrating Eq. (20) once with respect to y and using the condition

$$\frac{\partial\psi}{\partial y} = 0 \quad \text{and} \quad \frac{\partial u}{\partial y} = 0 \quad \text{at} \quad y = H, \tag{21}$$

we have

$$0 = -\frac{dp}{dx}(y - H) + \eta\frac{\partial u}{\partial y} - \varepsilon\frac{\partial\psi}{\partial y}E_S. \tag{22}$$

Integrating once again from $y = 0$ to a general point, we have, after setting $u\,(y = 0) = 0$,

$$u = \frac{dp}{dx}\int_0^y \frac{Y - H}{\eta}d\xi + E_S\int_0^y \frac{\varepsilon}{\eta}\frac{\partial\psi}{\partial Y}dY,$$

or,

$$u = -\frac{H^2}{2\eta_l}\frac{dp}{dx}\tilde{u}_p + \frac{\varepsilon_l\zeta E_S}{\eta_l}\tilde{u}_E, \tag{23}$$

where Y is a dummy variable used to represent the integration to the general point y. In Eq. (23),

$$\tilde{u}_p = \int_0^{\tilde{y}} 2\frac{1 - \tilde{Y}}{\tilde{\eta}}d\tilde{Y}, \tag{24}$$

and

$$\tilde{u}_E = \int_0^{\tilde{y}} \frac{\tilde{\varepsilon}}{\tilde{\eta}\tilde{\zeta}}\frac{\partial\tilde{\psi}}{\partial\tilde{Y}}d\tilde{Y}, \tag{25}$$

where $\tilde{Y} = Y/H$, $\tilde{\eta} = \eta/\eta_l$, and $\tilde{\zeta} = ez\zeta/k_BT$.

The condition for finding the as-yet-unknown value of the streaming potential field is that the total ionic current across the cross section must be zero [97]:

$$I = ez\int_0^{2H}(n_+u_+ - n_-u_-)\,dy = 0, \tag{26}$$

from which we obtain

$$\tilde{E}_S = \frac{E_S}{E_0} = \frac{I_1}{I_2 + \bar{R}I_3}, \tag{27}$$

where

$$E_0 = -\frac{fH^2}{2ez\eta_l}\frac{dp}{dx}, \tag{28}$$

$$I_1 = \int_0^2 \sinh(\tilde{\psi})\tilde{u}_p d\tilde{y}, \tag{29}$$

$$I_2 = \int_0^2 \cosh(\tilde{\psi})d\tilde{y}, \tag{30}$$

$$I_3 = \frac{\tilde{\zeta}}{4}\int_0^2 \sinh(\tilde{\psi})\tilde{u}_E d\tilde{y}, \tag{31}$$

and

$$\bar{R} = \frac{4f\varepsilon_l k_BT}{e^2z^2\eta_l}. \tag{32}$$

Using these in the expression of the velocity from Eq. (23) we have

$$\tilde{u} = \tilde{u}_p - \tfrac{1}{4}\bar{R}\tilde{\zeta}\tilde{E}_S\tilde{u}_E, \tag{33}$$

where u has been nondimensionalized by $(-\frac{H^2}{2\eta_l}\frac{dp}{dx})$.

The gross effect of the streaming potential is to retard the flow. This might be viewed as an effective increase in viscosity. To study this, we find an expression for the effective viscosity considering only a pressure-gradient driven flow (with no electrokinetic effects) that gives the same volumetric flow rate as that due to the velocity profile in Eq. (33). Thus, equating the volumetric flow rates we have

$$-\frac{H^2}{2\eta_l}\frac{dp}{dx}\int_0^2 \tilde{u}\,d\tilde{y} = \int_0^2 \tilde{u}_{PG}d\tilde{y},$$

where $\tilde{u}_{PG} = -\frac{H^2}{2\eta_{\text{eff}}}\frac{dp}{dx}(2\tilde{y} - \tilde{y}^2)$, so that

$$\tilde{\eta}_{\text{eff}} = \frac{\eta_{\text{eff}}}{\eta_l} = \frac{4}{3\tilde{Q}}, \tag{34}$$

where $\tilde{Q} = \int_0^2 \tilde{u}\,d\tilde{y}$.

III. RESULTS AND DISCUSSIONS

In this section, we first present a typical profile of the order parameter variable, and then study the overall flow structure in terms of the normalized effective velocity from Eq. (34), looking at its variation with the degree of hydrophobicity (represented in terms of the contact angle value), and delineating the interplay between the length scale of the EDL structure and that of the hydrophobicity mediated depletion. For the generation of our results we fix the values of $\rho_{\text{ratio}} = \rho_v/\rho_l$ at 0.001, $\varepsilon_{\text{ratio}} = \varepsilon_v/\varepsilon_l$ at 0.8 (following Le and Zhang [93]) and $\eta_{\text{ratio}} = \eta_v/\eta_l$ at 1/3 (following Andrienko *et al.* [71]).

We illustrate a typical instance of the variation in the order parameter variable ϕ in the direction normal to the wall. For this, we choose $\beta = 1$ [54,69,70] and $\epsilon^2 = (\xi/H)^2 = 0.01$. From the profile in Fig. 1, we observe that the value of ϕ decreases from the surface value, ϕ_S, that corresponds to $\theta_w = 140^\circ$, and smoothly transitions into the bulk undepleted liquid value ($\phi = -1$). We also observe the variation of the surface value ϕ_S with the contact angle θ_w in the inset of Fig. 1. The higher the value of ϕ_S (corresponding to higher values of the contact angle), the closer the region just adjacent to the surface is to the "bulk" vapor value. This is consistent with progressively stronger hydrophobic effects of the wall with increasing value of the contact angle.

Figures 2(a)–2(d) show the variation of the effective viscosity normalized by the bulk value of the liquid viscosity, $\tilde{\eta}_{\text{eff}} = \eta_{\text{eff}}/\eta_l$ with the contact angle corresponding to the values $K = 5$, 10, 25, 50, each panel showing the variations for two different values of the nondimensional zeta potential, $\tilde{\zeta} = -1, -4$. The general trend observed in all the panels is that the effective viscosity decreases for both values of the nondimensional zeta potential with increasing value of the contact angle, i.e., with stronger hydrophobic effects. This may be clearly attributed to the fact that such stronger hydrophobic effects lead to stronger depletion of the liquid from the interfacial region. It is important to note that "stronger

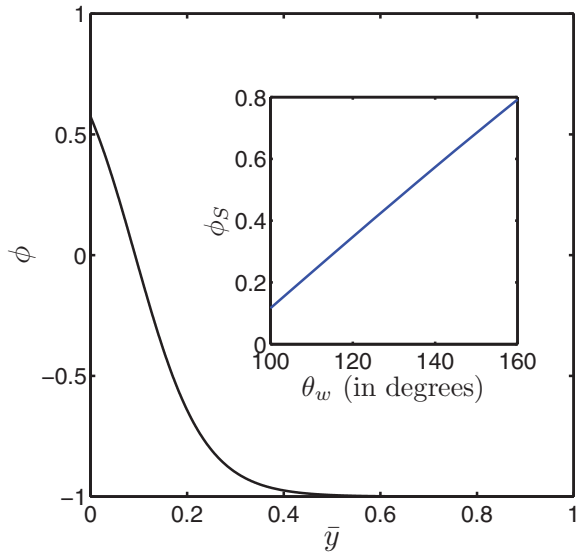

FIG. 1. (Color online) Variation of the phase-field variable ϕ in the direction normal to the wall for $\theta_w = 140^\circ$ and $\epsilon^2 = (\xi/H)^2 = 0.01$. The inset shows how the wall boundary condition for ϕ varies with increasing values of the contact angle which in turn represent higher degrees of hydrophobicity of the substrate.

depletion" does not mean that the extent of the depleted region increases with increase in the value of the contact angle. Rather, as shown in Fig. 1, higher contact angle value implies higher value of ϕ_S indicating that the region just adjacent to the wall becomes progressively closer to the bulk vapor region. That is, within the same length scale of the depletion, the effects of the bulk vapor with lower viscosity become more pronounced. It is this stronger depletion with higher values of the contact angle that leads to lower overall resistances to the fluid flow.

Beyond this, we note two subtle points which may be observed across the four panels. First, it is only for the first two panels (corresponding to $K = 5$, 10) that the normalized effective viscosity shows values higher than 1 for certain regimes. Second, the discrepancy between the values of the effective normalized viscosity for $\tilde{\zeta} = -1$ and $\tilde{\zeta} = -4$ become gradually smaller as the value of K increases from panel (a) to panel (d). To explain these observations, it is important to consider the values of K in concert with the value of H/ξ. Indeed, for the entire set of results shown in Fig. 2, the value of H/ξ is kept fixed at 10. This immediately indicates that there are three distinct regimes of interest shown in the four panels. In Fig. 2(a), $K = H/\lambda_l = 5$, implying $\lambda_l > \xi$. This means that the characteristic thickness of the EDL is higher than the depleted region length scale. In contrast, for Fig. 2(b), we have $K = H/\lambda_l = 10$ implying $\lambda_l = \xi$. In Figs. 2(c) and 2(d), however, we have $K = H/\lambda_l = 25$, 50, respectively, implying that for both these cases, $\lambda_l < \xi$. It is the interplay between the two length scales which gives rise to the two subtle observations pointed out earlier. When the length scale of the EDL is higher than that of the depleted region, the electrokinetic effects have a tendency to dominate. This is particularly manifested in Fig. 2(a) corresponding to the higher value of the zeta potential ($\tilde{\zeta} = -4$), as attributed to a well-established fact that streaming potential effects become progressively stronger with higher values of the zeta potential. Thus, for the entire regime of the contact angle (from 110° to 160°), the normalized effective viscosity is higher than 1 indicating that the inhibition to the flow arising from the electrokinetic component of the flow overwhelms whatever little decrease in flow resistance is offered by the depleted region. It is, of course, noteworthy that for $\tilde{\zeta} = -1$ when the streaming potential effects are relatively weaker, even the higher extent of the EDL is not sufficient to overwhelm the hydrophobic effects, and that results in values of the normalized effective viscosity being less than 1 for all values of the contact angle.

Figure 2(b) shows a clear manifestation of the aforementioned interplay between the length scales of the EDL and the depleted region, corresponding to the case with $\tilde{\zeta} = -4$. For relatively lower values of the contact angle, the electrokinetic effects continue to overwhelm the hydrophobic effects as in the previous case. However, beyond $\theta_w \sim 140^\circ$, the normalized effective viscosity falls below unity. This means that when the length scales of the EDL and the depleted region are equal, the sensitive interplay between them gets manifested such that for sufficiently high value of the contact angle, the hydrophobic effects countervail the inhibiting influence of the streaming potential. A value of $\tilde{\eta}_{\text{eff}}$ less than 1 means that even though the back electrokinetic flow induced by the streaming potential field may be present, from the perspective of the overall flow rate, the effective resistance to the fluid is still less than what it would have been had there been only a pressure-gradient driven flow with no hydrophobicity-induced depletion. Again, just as in Fig. 2(a), the relatively weaker influence of the streaming potential corresponding to $\tilde{\zeta} = -1$ ensures that $\tilde{\eta}_{\text{eff}}$ is less than 1 throughout.

In contrast, for Figs. 2(c) and 2(d), the length scale of the EDL is less than that of the depleted region. This ensures that the hydrophobic effects are consistently manifested in being more resistant to the inhibiting effects of the streaming potential so that the value of the effective normalized viscosity, $\tilde{\eta}_{\text{eff}}$ is less than 1 in the entire regime of interest of the contact angle and for both values of the dimensionless zeta potential, $\tilde{\zeta} = -1$, 4.

The second observation that the discrepancy in the values of the effective normalized viscosity for $\tilde{\zeta} = -1$ and $\tilde{\zeta} = -4$ becomes progressively smaller from Fig. 2(a) to Fig. 2(d) can be easily explained again on the basis of the interplay between the length scales of the EDL and the depleted region. When $\lambda_l > \xi$ [Fig. 2(a)], the influence of the electrokinetic effects due to the streaming potential are relatively stronger than the hydrophobic effects. So, even though the hydrophobic effects are strong enough to countervail the inhibiting influence for $\tilde{\zeta} = -1$ (manifested in $\tilde{\eta}_{\text{eff}}$ being less than 1), the distinction between $\tilde{\zeta} = -1$ and $\tilde{\zeta} = -4$ is pronounced. As the EDL length scale decreases in the other three panels, it is the influence of the hydrophobic effects that start taking precedence over the electrokinetic effects. Although differences between $\tilde{\zeta} = -1$ and $\tilde{\zeta} = -4$ do get manifested, such differences are progressively smaller indicating that the overall flow tends towards a situation where the sole effect on the primary pressure-gradient driven flow is that due to the hydrophobicity-induced depletion.

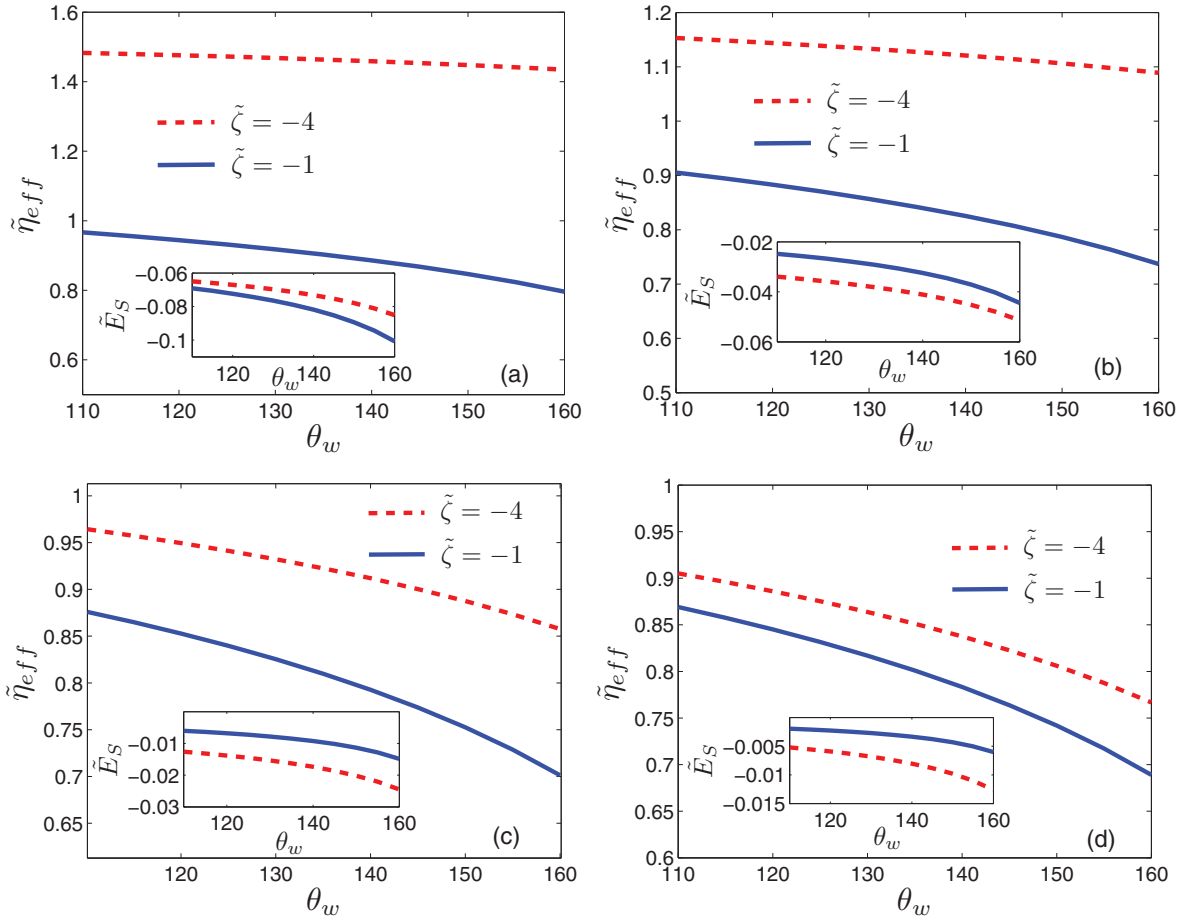

FIG. 2. (Color online) Variation of the effective viscosity normalized by the bulk liquid viscosity, $\tilde{\eta}_{\text{eff}} = \eta_{\text{eff}}/\eta_l$, with the contact angle for $\tilde{\zeta} = -1$ (represented by the blue solid lines), and $\tilde{\zeta} = -4$ (represented by the red dashed lines) corresponding to $K = 5$, 10, 25, 50, respectively, in panels (a)–(d). The insets in each panel show the variation of the dimensionless streaming potential field with the contact angle.

Another important observation relates to the insets of Figs. 2(a)–2(d) where the variation of the nondimensional streaming potential field is shown corresponding to the same regime of the contact angle for which the effective normalized viscosities are shown, and also for the same two values of the dimensionless zeta potential. The critical thing to note is that while in Fig. 2(a) the value of the nondimensional streaming potential field corresponding to $\tilde{\zeta} = -1$ is higher in magnitude than the one corresponding to $\tilde{\zeta} = -4$, in Figs. 2(b)–2(d), the trend is consistently opposite. This might apparently indicate that the streaming potential effects should have been weaker for $\tilde{\zeta} = -4$ compared to $\tilde{\zeta} = -1$. However, such a possibility is precluded by the fact that in the expression of the dimensionless velocity component due to the streaming potential effects [Eq. (25)], the distribution of the electrokinetic potential (associated with the distribution of the ions) has a strong role to play. Thus, in the expression of the overall velocity, Eq. (33), there is the influence of the streaming potential field as well as that of this potential distribution that determines the structure of the EDL. Since the influence of this latter potential distribution (associated with the ionic distribution in the EDL) propagates more into the bulk for $\tilde{\zeta} = -4$ than for $\tilde{\zeta} = -1$, the overall electrokinetic effects are indeed stronger for $\tilde{\zeta} = -4$. Interestingly, this discussion again points to the paramount importance that the length scale of the EDL has in determining the overall character of the flow.

An additional important point to note regarding the insets in Fig. 2 is that the magnitude of the streaming potential field increases corresponding to both $\tilde{\zeta} = -1$ and $\tilde{\zeta} = -4$ as the value of the contact angle increases. This increasing trend is again in apparent conflict with the decreasing trend of the effective normalized viscosity from which one might naïvely assume that the streaming potential field should have been progressively weaker. This, however, may be easily explained if we note that the higher hydrophobicity implied by higher values of the contact angle ensure that the bulk vapor value is more strongly manifested in the wall-adjacent region. Thus, even with the length scales held fixed, the degree of hydrophobicity has a distinctive influence in determining the overall character of the flow. This reasoning is a close counterpart of the transitioning trend of $\tilde{\eta}_{\text{eff}}$, changing from values higher than 1 to lower than 1, observed in Fig. 2(b) corresponding to the case of $\tilde{\zeta} = -4$. The higher values of the streaming potential field with increase in the value of the contact angle can be easily explained on the basis of the fact that higher hydrophobicity leads to augmentations in the base flow (driven by the pressure gradient) which, in turn, results in higher streaming current of the ions. Since the

streaming potential field directly (and strongly) depends on this streaming current, its magnitude increases with increasing hydrophobicity.

IV. CONCLUSIONS

In this study, we have attempted to capture the effects of hydrophobicity on streaming potential mediated flows through narrow conduits. In a clear departure from prior studies where hydrophobic effects are relegated to the boundary through the specification of a slip length, we have presented a phase-field model to capture the realistic picture of hydrophobicity-induced depletion of the fluid in the wall-adjacent region. This depletion is represented through the phase-field variable (alternatively, termed as order parameter). The viscosity and the permittivity are expressed in terms of this order parameter so that the smooth variations in these physicochemical parameters are realistically captured. These smooth variations are then incorporated in the framework for the determination of the streaming potential field and the velocity arising as a combined consequence of the primary pressure-gradient drive and the self-consistently induced streaming potential. Since the overall effect of the streaming potential is to inhibit the pressure-gradient driven flow (known as the electroviscous effect), and since the total volumetric flow rate is of tremendous importance in practical devices, we express the gross nature of the flow in terms of an effective viscosity that would result in the same (reduced) volumetric flow rate had there been only a pressure-gradient driven flow (with no electrokinetic effects). The variations of this effective viscosity (normalized by the bulk liquid viscosity) with the contact angle (representing the degree of hydrophobicity of the wall) unveil a sensitive interplay between the length scale of the EDL structure and that of the hydrophobicity-induced depletion. Of particular importance to note is that prior to our investigation, it had not been possible to study such interplays, particularly in the context of streaming potential mediated flows. We expect that this study will be an important step forward in more realistic modeling of streaming potential mediated flows, especially as the characteristic dimension of the confinements goes down to the submicron and even nanometric scales. We also hope that it will help in the design of practical devices, particularly those concerned with electrokinetic energy conversion.

[1] R. J. Hunter, *Foundations of Colloid Science*, 2nd ed. (Oxford University Press, New York, 2001).

[2] A. V. Delgado, F. González-Caballero, R. J. Hunter, L. K. Koopal, and J. Lyklema, J. Colloid Interface Sci. **309**, 194 (2007).

[3] A. M. Gallardo-Moreno, V. Vadillo-Rodríguez, J. Perera-Núñez, J. M. Bruque, and M. L. González-Martín, Phys. Chem. Chem. Phys. **14**, 9758 (2012).

[4] J. H. Saunders, M. D. Jackson, and C. C. Pain, Geophys. Res. Lett. **33**, L15316 (2006).

[5] P. M. Reppert, Ph.D. thesis, Massachusetts Institute of Technology, 2000, http://dspace.mit.edu/handle/1721.1/8851

[6] A. Revil, P. A. Pezard, and P. W. J. Glover, J. Geophys. Res. **104**, 20021 (1999).

[7] A. Revil, H. Schwaeger, L. M. Cathles III, and P. D. Manhardt, J. Geophys. Res. **104**, 20033 (1999).

[8] S. R. Pollack, N. Petrov, R. Saltzstein, G. Brankov, and R. Blagoeva, J. Biomech. **17**, 627 (1984).

[9] R. C. Riddle and H. J. Donahue, J. Orthop. Res. **27**, 143 (2009).

[10] A. C. Ahn and A. J. Grodzinsky, Med. Eng. Phys. **31**, 733 (2009).

[11] M. Nyström, A. Pihlajamäki, and N. Ehsani, J. Membr. Sci. **87**, 245 (1994).

[12] M. Pontie, X. Chasseray, D. Lemordant, and J. M. Lainé, J. Membr. Sci. **129**, 125 (1997).

[13] T. G. M. van de Ven, P. Warszynski, and S. S. Dukhin, J. Colloid Interface Sci. **157**, 328 (1993).

[14] S. G. Bike, L. Lazarro, and D. C. Prieve, J. Colloid Interface Sci. **175**, 411 (1995).

[15] S. G. Bike and D. C. Prieve, J. Colloid Interface Sci. **175**, 422 (1995).

[16] P. Warszyski, X. Wu, and T. van de Ven, Colloids Surf. A **140**, 183 (1998).

[17] S. M. Tabatabaei, T. G. M. van de Ven, and A. D. Rey, J. Colloid Interface Sci. **301**, 291 (2006).

[18] O. Schnitzer, I. Frankel, and E. Yariv, Math. Modell. Nat. Phenom. **7**, 64 (2012).

[19] E. Yariv, O. Schnitzer, and I. Frankel, J. Fluid Mech. **685**, 306 (2011).

[20] O. Schnitzer, I. Frankel, and E. Yariv, J. Fluid Mech. **704**, 109 (2012).

[21] J. Chakraborty and S. Chakraborty, Phys. Fluids **22**, 122002 (2010).

[22] J. Chakraborty and S. Chakraborty, Phys. Fluids **23**, 082004 (2011).

[23] H. Daiguji, P. Yang, A. J. Szeri, and A. Majumdar, Nano Lett. **4**, 2315 (2004).

[24] F. H. J. van der Heyden, D. J. Bonthuis, D. Stein, C. Meyer, and C. Dekker, Nano Lett. **6**, 2232 (2006).

[25] F. H. J. van der Heyden, D. J. Bonthuis, D. Stein, C. Meyer, and C. Dekker, Nano Lett. **7**, 1022 (2007).

[26] C. L. A. Berli, J. Colloid Interface Sci. **349**, 446 (2010).

[27] C.-C. Chang and R.-J. Yang, Appl. Phys. Lett. **99**, 083102 (2011).

[28] A. Bandopadhyay and S. Chakraborty, Langmuir **27**, 12243 (2011); Appl. Phys. Lett. **101**, 043905 (2012).

[29] A. Bandopadhyay, J. Dhar, and S. Chakraborty, Phys. Rev. E **88**, 033014 (2013).

[30] R. F. Probstein, *Physicochemical Hydrodynamics*, 2nd ed. (Wiley-Interscience, Hoboken, NJ, 2003).

[31] E. Lauga, M. Brenner, and H. Stone, in *Springer Handbook of Experimental Fluid Mechanics*, edited by C. Tropea, A. L. Yarin, and J. F. Foss (Springer, Berlin, Heidelberg, 2007), pp. 1219–1240.

[32] L. Bocquet and J.-L. Barrat, Soft Matter **3**, 685 (2007).

[33] J. Eijkel, Lab Chip **7**, 299 (2007).

[34] L. Bocquet and E. Charlaix, Chem. Soc. Rev. **39**, 1073 (2010).

[35] O. I. Vinogradova and A. V. Belyaev, J. Phys.: Condens. Matter **23**, 184104 (2011).

[36] F. H. Stillinger, J. Solution Chem. **2**, 141 (1973).
[37] C.-Y. Lee, A. McCammon, and P. J. Rossky, J. Chem. Phys. **80**, 4448 (1984).
[38] K. Lum, D. Chandler, and J. D. Weeks, J. Phys. Chem. B **103**, 4570 (1999).
[39] R. Steitz, T. Gutberlet, T. Hauss, B. Klosgen, R. Krastev, S. Schemmel, A. C. Simonsen, and G. H. Findenegg, Langmuir **19**, 2409 (2003).
[40] D. Schwendel, T. Hayashi, R. Dahint, A. Pertsin, M. Grunze, R. Steitz, and F. Schreiber, Langmuir **19**, 2284 (2003).
[41] D. A. Doshi, E. B. Watkins, J. N. Israelachvili, and J. Majewski, Proc. Natl. Acad. Sci. USA **102**, 9458 (2005).
[42] M. Mezger, H. Reichert, S. Schoder, J. Okasinski, H. Schroder, H. Dosch, D. Palms, J. Ralston, and V. Honkimaki, Proc. Natl. Acad. Sci. USA **103**, 18401 (2006).
[43] M. Maccarini, R. Steitz. M. Himmelhaus, J. Fick, S. Tatur, M. Wolff, M. Grunze, J. Janecek, and R. Netz, Langmuir **23**, 598 (2007).
[44] J. Janecek and R. R. Netz, Langmuir **23**, 8417 (2007).
[45] F. Sedlmeier, J. Janecek, C. Sendner, L. Bocquet, R. R. Netz, and D. Horinek, Biointerphases **3**, FC23 (2008).
[46] M. Mezger, F. Sedlmeier, D. Horinek, H. Reichert, D. Pontoni, and H. Dosch, J. Am. Chem. Soc. **132**, 6735 (2010).
[47] S. Chattopadhyay, A. Uysal, B. Stripe, Y.-g. Ha, T. J. Marks, E. A. Karapetrova, and P. Dutta, Phys. Rev. Lett. **105**, 037803 (2010).
[48] M. Walz, S. Gerth, P. Falus, M. Klimczak, T. H. Metzger, and A. Magerl, J. Phys.: Condens. Matter **23**, 324102 (2011).
[49] J. Israelachvili, *Intermolecular and Surface Forces* (Academic, Amsterdam, 2003).
[50] C. I. Bouzigues, P. Tabeling, and L. Bocquet, Phys. Rev. Lett. **101**, 114503 (2008).
[51] M.-C. Audry, A. Piednoir, P. Joseph, and E. Charlaix, Faraday Discuss. **146**, 113 (2010).
[52] L. Joly, C. Ybert, E. Trizac, and L. Bocquet, Phys. Rev. Lett. **93**, 257805 (2004).
[53] D. M. Huang, C. Sendner, D. Horinek, R. R. Netz, and L. Bocquet, Phys. Rev. Lett. **101**, 226101 (2008).
[54] S. Chakraborty, Phys. Rev. Lett. **100**, 097801 (2008).
[55] V. M. Muller, I. P. Sergeeva, V. D. Sobolev, and N. V. Churaev, Colloid J. USSR **48**, 606 (1986).
[56] J. Yang and D. Y. Kwok, Langmuir **19**, 1047 (2003).
[57] J. Yang and D. Y. Kwok, Anal. Chim. Acta **507**, 39 (2004).
[58] A. Ajdari and L. Bocquet, Phys. Rev. Lett. **96**, 186102 (2006).
[59] L. Joly, C. Ybert, E. Trizac, and L. Bocquet, J. Chem. Phys. **125**, 204716 (2006).
[60] D. M. Huang, C. Cottin-Bizonne, C. Ybert, and L. Bocquet, Phys. Rev. Lett. **101**, 064503 (2008).
[61] T. M. Squires, Phys. Fluids **20**, 092105 (2008).
[62] V. Tandon and B. J. Kirby, Electrophoresis **29**, 1102 (2008).
[63] A. V. Belyaev and O. I. Vinogradova, Phys. Rev. Lett. **107**, 098301 (2011).
[64] P. Goswami and S. Chakraborty, Microfluid Nanofluid **11**, 255 (2011).
[65] S. Pennathur, J. C. T. Eijkel, and A. van den Berg, Lab Chip **7**, 1234 (2007).
[66] Y. Ren and D. Stein, Nanotechnology **19**, 195707 (2008).
[67] P. Goswami and S. Chakraborty, Langmuir **26**, 581 (2010).
[68] C. Tretheway and C. D. Meinhart, Phys. Fluids **16**, 1509 (2004).
[69] J. Chakraborty, S. Pati, S. K. Som, and S. Chakraborty, Phys. Rev. E **85**, 046305 (2012); see also K. Chaudhury, U. Ghosh, and S. Chakraborty, Int. J. Heat Mass Transfer **67**, 1083 (2013).
[70] S. Chakraborty, Phys. Rev. Lett. **99**, 094504 (2007).
[71] D. Andrienko, B. Dünweg, and O. I. Vinogradova, J. Chem. Phys. **119**, 13106 (2003).
[72] J. W. Cahn, J. Chem. Phys. **66**, 3667 (1977).
[73] V. E. Badalassi, H. D. Ceniceros, and S. Banerjee, J. Comput. Phys. **190**, 371 (2003).
[74] D. Jasnow and D. Viñals, Phys. Fluids **8**, 660 (1996).
[75] D. Jacqmin, J. Comput. Phys. **155**, 96 (1999).
[76] O. Kuksenok and A. C. Balazs, Phys. Rev. E **68**, 011502 (2003).
[77] O. Kuksenok, D. Jasnow, and A. C. Balazs, Phys. Rev. E **68**, 051505 (2003).
[78] O. Kuksenok, D. Jasnow, and A. C. Balazs, Phys. Rev. Lett. **95**, 240603 (2005).
[79] P. Yue, J. J. Feng, C. Liu, and J. Shen, J. Fluid Mech. **515**, 293 (2004).
[80] V. V. Khatavkar, P. D. Anderson, and H. E. H. Meijer, J. Fluid Mech. **572**, 367 (2007).
[81] O. A. Folovskaya, A. A. Nepomnyashchy, A. Oron, and A. A. Golovin, Phys. Fluids **20**, 112105 (2008).
[82] U. Thiele, S. Madruga, and L. Frastia, Phys. Fluids **19**, 122106 (2007).
[83] S. Madruga and U. Thiele, Phys. Fluids **21**, 062104 (2009).
[84] S. Madruga and U. Thiele, Eur. Phys. J.: Spec. Top. **192**, 101 (2011).
[85] L.-Q. Chen, Annu. Rev. Mater. Res. **32**, 113 (2002).
[86] D. Bonn and D. Ross, Rep. Prog. Phys. **64**, 1085 (2001).
[87] L. M. Pismen and Y. Pomeau, Phys. Rev. E **62**, 2480 (2000).
[88] R. J. LeVeque, *Finite Difference Methods of Ordinary and Partial Differential Equations* (SIAM, Philadelphia, PA, 2007).
[89] H. Ding and P. D. M. Spelt, Phys. Rev. E **75**, 046708 (2007).
[90] H. Ding, P. D. M. Spelt, and C. Shu, J. Comput. Phys. **226**, 2078 (2007).
[91] R. Borcia and M. Bestehorn, Eur. Phys. J. B **44**, 101 (2005).
[92] J. Park, X.-Q. Feng, and W. Lu, J. Appl. Phys. **109**, 034309 (2011).
[93] G. Le and J. Zhang, Langmuir **27**, 5366 (2011).
[94] N. Mishchuk, J. Colloid Interface Sci. **320**, 599 (2008).
[95] N. Mishchuk, Adv. Colloid Interface Sci. **168**, 149 (2011).
[96] S. V. Patankar, *Numerical Heat Transfer and Fluid Flow* (Taylor & Francis, Kundli, India, 2004).
[97] S. Chakraborty and S. Das, Phys. Rev. E **77**, 037303 (2008).